Check for updates

Perspectives for the conversion of perovskite indoor photovoltaics into IoT reality

Xinyi Zhu,†[a] Jie Xu,†[b] Hanlin Cen, [ID] [a] Zhaoxin Wu, [ID] *[a,c] Hua Dong [ID] *[a,c] and Jun Xi [ID] *[a]

As a competitive candidate for powering low-power terminals in Internet of Things (IoT) systems, indoor photovoltaic (IPV) technology has attracted much attention due to its effective power output under indoor light illumination. One such emerging photovoltaic technology, perovskite cell, has become a hot topic in the field of IPVs due to its outstanding theoretical performance limits and low manufacturing costs. However, several elusive issues remain limiting their applications. In this review, the challenges for perovskite IPVs are discussed in view of the bandgap tailoring to match indoor light spectra and the defect trapping regulation throughout the devices. Then, we summarize up-to-date perovskite cells, highlighting advanced strategies such as bandgap engineering, film engineering and interface engineering to enhance indoor performance. The investigation of indoor applications of large and flexible perovskite cells and integrated devices powered by perovskite cells is exhibited. Finally, the perspectives for the perovskite IPV field are provided to help facilitate the further improvement of indoor performance.

[a]*Key Laboratory for Physical Electronics and Devices of the Ministry of Education & Shaanxi Key Lab of Information Photonic Technique, School of Electronic Science and Engineering, Xi'an Jiaotong University, No. 28, Xianning West Road, Xi'an, 710049, China. E-mail: zhaoxinwu@mail.xjtu.edu.cn, donghuaxjtu@mail.xjtu.edu.cn, jun.xi@xjtu.edu.cn*
[b]*School of Science, Xi'an University of Architecture and Technology, Xi'an, 710055, China*
[c]*Collaborative Innovation Center of Extreme Optics, Shanxi University, Taiyuan 030006, China*
†These authors contributed equally.

Introduction

In recent years, with the rapid development of Big Data and Internet of Things (IoT), numerous smart products such as sensors, remote actuators and communication devices have been fabricated and applied under different conditions to meet the demands of data monitoring and transmission, almost half of which may be indoor.[1–4] Though these IoT devices have exhibited ultra-low power consumption, effective power supply for billions of devices remains a serious impediment for the deeper deployment of IoT, since

Xinyi Zhu received his BS in Materials Science and Engineering from Wuhan University of Technology in 2019. He is currently a PhD student in Electronic Science and Technology at Xi'an Jiaotong University. His research interests are focused on the large-area flexible perovskite modules and the indoor perovskite photovoltaics.

Xinyi Zhu

Jie Xu received her PhD degree in Electronic Science and Technology under the supervision of Profs. Hua Dong and Zhao-Xin Wu from Xi'an Jiaotong University, China, in 2021. Currently, she is the associate professor in the Xi'an University of Architecture and Technology. Her primary research interest is focused on organic–inorganic hybrid perovskite photovoltaic materials and devices for outdoor and indoor applications.

Jie Xu
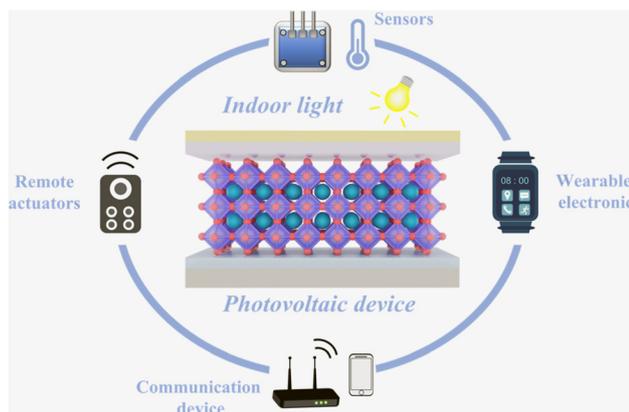
Fig. 1 Various IoT devices powered by photovoltaic devices under indoor light illumination.

traditional battery power supply cannot meet the new requirements regarding lightweight, high efficiency and low cost.[5–7] As shown in Fig. 1, considering the characteristics of indoor conditions and the benefit of photovoltaics, it is rational to replace the batteries with indoor photovoltaics (IPVs) to achieve self-powered integrated products, which is beneficial for the long-term working stability of IoT systems.[8–11]

For IPV application, various materials as absorbing layers have been employed to achieve good performance under indoor conditions.[12–16] The earliest application may originate from amorphous silicon, which powered pocket calculators. However, Si-based cells exhibit inferior efficiency under indoor light illumination due to the mismatch between their narrow bandgaps and the spectrum of indoor lights.[17,18] As for the III–V semiconductor-based cells, the better spectrum match improves the indoor efficiency, but the high fabrication cost and strict growth conditions of materials seriously restrict their further commercial application.[19–21] Due to the fast development of photovoltaic technologies, the investigation of

IPVs may focus more on third-generation photovoltaic technologies including organic photovoltaics, dye-sensitized cells, and perovskite cells.[22–26]

Among these, the perovskite cells exhibit tremendous potential for high–indoor efficiency devices owing to the desirable optoelectronic characteristics such as tunable bandgap (ranging from 1.2 eV to about 3.5 eV), high optical absorption coefficients (10^5 cm^{-1}), small exciton binding energy (<100 meV) and long carrier diffusion length (over 1 μm).[27–29] Nowadays, the record indoor power conversion efficiency (PCE) of perovskite cells has exceeded 40% (under 1000 lux), which far exceeds other types of cells.[30–32] Moreover, the low crystallization energy barrier of perovskites facilitates low-temperature scalable fabrication processes including blade coating, slot-die coating, spray printing and inkjet printing, which can easily meet the demands of flexibility and practicality of different smart products.[33–36] Based on the excellent indoor performance and convenient fabrication process, perovskite IPVs exhibit promising prospects for further application in IoT systems.[37–39]

In this review, we discuss the underlying challenges for the indoor application of perovskite cells, and then summarize state-of-the-art strategies such as bandgap engineering of perovskites, the film engineering of perovskites, and the interface engineering of devices. Moreover, the current state of larger area and flexible perovskite cells and their practical application is introduced. Finally, this review provides an understanding of the carrier dynamics mechanism under indoor light illumination and new approaches for the indoor performance improvement of perovskite IPVs are suggested.

Characteristics of artificial lighting and perovskite IPVs

A variety of artificial lighting sources including light-emitting diodes (LED), incandescent lamps, halogen bulbs and fluo-

Hanlin Cen received his BS in Applied Physics from Xi'an Jiaotong University in 2022. He is currently a MA student in Electronic Science and Technology at Xi'an Jiaotong University. His research interests are focused on organic perovskite photovoltaic devices and indoor perovskite photovoltaics.

Hanlin Cen

Zhaoxin Wu is currently a tenured professor at Xi'an Jiaotong University. He was awarded the title of Distinguished Professor of the "TengFei Plan" of Xi'an Jiaotong University, "Outstanding Talents in the New Century" of the Ministry of Education, and the leader of Shaanxi Province in science and technology entrepreneurship. His research areas include organic–inorganic composite perovskite solar cells, new

Zhaoxin Wu

organic–inorganic electroluminescent displays and lighting devices, and organic laser semiconductor photovoltaic devices.
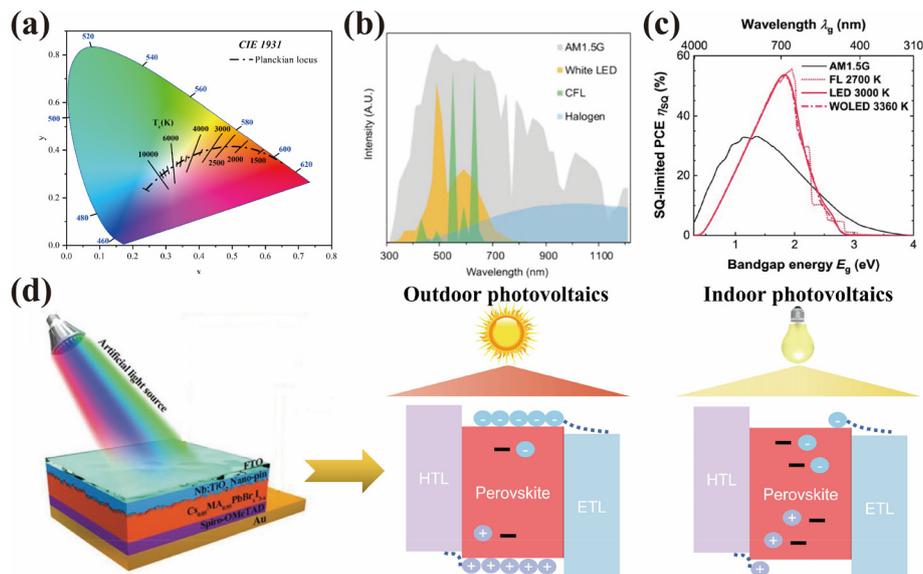
Fig. 2 (a) CIE 1931 chromaticity diagram (the curved perimeter indicates monochromatic light colors and black dotted line shows the color of a blackbody at different color temperatures). (b) Emission spectra of the solar spectrum (AM 1.5G), white LED, compact FL (CFL) and halogen bulb. Reproduced with permission from ref. 42. Copyright 2014, IEEE. (c) SQ limited PCE *vs.* bandgap energy (E_g) for the standard solar spectrum and three different artificial indoor light sources. Reproduced with permission from ref. 40. Copyright 2020, Elsevier Ltd. (d) Schematic diagram of carrier generation, recombination and transmission for outdoor and indoor perovskite cells.

rescent lamps (FL) have greatly promoted human civilization. In general, for any indoor artificial lighting, we can obtain the relative spectral power distributions, illuminance and color coordinates (the color coordinate corresponds to a specific color temperature, which is given by CIE 1931 chromaticity diagram shown in Fig. 2a).[40]

Under the irradiation of an artificial indoor light source, perovskite cells can convert the input power (P_{in}) into electric energy, which is expressed as output power (P_{out}). Since an indoor artificial light source is usually quantified by illumi-

nance L, P_{in} can be obtained by a simple calculation. The relationship between L and P_{in} is as follows:[41]

$$L = K_r P_{in} \int_{360\,nm}^{830\,nm} S_{norm}(\lambda) V(\lambda) d\lambda \tag{1}$$

where K_r = 683.002 lm W^{-1}, $V(\lambda)$ is the spectral light efficiency function, and K_r and $V(\lambda)$ represent the maximum spectral light efficiency and spectral sensitivity of human vision, respectively. Spectral distribution ($S(\lambda)$) and illuminance (L)

Hua Dong

Hua Dong is currently a tenured associate professor at Xi'an Jiaotong University. He is the deputy director of Shaanxi Province Key Laboratory of Information Photonics Technology of China; senior member of the Optical Society of China; vice chairman of the National Young Optics Academic Forum of China. His research areas include advanced photovoltaic materials, semiconductor photovoltaic devices, and indoor photovoltaic technology. He has published more than 70 papers with more than 2500 citations and an H-index of 31.

Jun Xi

Jun Xi is currently an associate professor at Xi'an Jiaotong University. He completed his PhD at the same institution, and then started his postdoctoral work at the Global Frontier Center for Multiscale Energy System in Seoul National University with Prof. Mansoo Choi, and continued the research with Prof. Maria A. Loi in Photophysics and OptoElectronics Group, University of Groningen. His research interests cover from hybrid semiconductor design to optoelectronic device applications. He has authored 44 publications and earned more than 2000 citation times.

level can be measured using a spectrophotometer and a standard illuminance meter, respectively. According to eqn (1), we can calculate P_{in} as a function of L and $(S(\lambda))$, which is defined as a fixed constant given an artificial light source.[38]

The PCE of perovskite cells can be expressed as follows:

$$PCE = \frac{P_{out}}{P_{in}} \times 100\%. \qquad (2)$$

Therefore, the following two aspects should be paid attention to improve the PCE of perovskite cells:

(1) From the optical spectral matching viewpoint, wide bandgap perovskite materials should be chosen to maximize the matching degree of the emission spectrum of the artificial indoor light source, which makes the PCE closer to the Shockley–Queisser (SQ) limited efficiency. Fig. 2b shows the $(S(\lambda))$ of the solar spectrum (AM 1.5G), white LED, CFL, and halogen bulb.[42] The SQ-limited efficiencies for the standard solar spectrum and three different artificial indoor light sources are summarized in Fig. 2c. For these three artificial indoor sources under 300 lux, the optimal E_g value is 1.82–1.96 eV, and the maximum PCE reaches 57%.[40] This is due to the narrow and concentrated distribution of the artificial light spectrum.

(2) The illumination range of common artificial lighting is 100–1000 lux, and its incident power intensity ($\sim$100 μW cm^{-2}) is only 10^{-3} standard sunlight ($\sim$100 mW cm^{-2}).[40] From the perspective of the electrical behavior of the device, compared with outdoor sunlight, indoor artificial light sources should produce a lower concentration of free photogenerated carriers (Fig. 2d), which significantly limits photogenerated current density (J_{ph}).

In general, the key device parameters are closely associated, described as follows:[23,43]

$$J_{sc} = J_{ph} - J_0 \left[\exp\left(\frac{q(V + J_{sc}R_s)}{nk_BT} \right) - 1 \right] \\ - \frac{V + J_{sc}R_s}{R_{sh}} \qquad (3)$$

$$J_0 = qSne\Delta E_F/k_BT + J_{leak} \qquad (4)$$

$$V_{oc} = \frac{nKT}{q} \ln\left[\frac{I_{ph}(V_{oc})}{I_0} + 1 - \frac{V_{oc}}{R_{sh}I_0} \right] \qquad (5)$$

where J_0 is the dark current density, q is the elementary charge, k_B is the Boltzmann constant, T is the cell temperature, n is the ideal factor, S is the defect state density, ΔE_F is the potential difference between the quasi-Fermi levels, J_{leak} is the leakage current density, I_{ph} is the photogenerated current and I_0 is the dark saturation current.

The low series resistance (R_s) and extremely high shunt resistance (R_{sh}) with ultra-low leakage current are the two main factors to improve the short-circuit current density (J_{sc}), as observed from eqn (3) and (4), which are also related to the density of defect states within the functional layer and the different interfaces. According to eqn (5), the relatively fewer recombination losses and higher R_{sh} lead to increased open-circuit voltage (V_{oc}), and hence a higher PCE.

Therefore, for perovskite cells operating under typical artificial light sources, the efficiency improvement is designed optically electrically with both behavioral regulations. The focus of the relevant key issues differs from outdoor photovoltaic devices. The currently reported indoor efficiency records for perovskite cells are still far from the SQ theoretical limit. In principle, the desired PCE can be obtained by tuning the absorption spectrum, reducing V_{oc} losses by reducing the trap density and maximizing R_{sh} by reducing the leakage current.

Development of perovskite cells for indoor applications

Due to the superior characteristics of perovskite materials, great attention has been paid to the research of perovskite cells.[44–47] Though the early investigation may focus more on the outdoor performance of devices, recent research shows more concern for indoor performance owing to the rapid development of IoT systems.[48–50] The first investigation on perovskite IPVs was conducted by Kawata *et al.* in 2015, demonstrating a device that achieved 19.8% PCE at 1000 lux.[51] Soon in a few years, the indoor PCE of perovskite cells has exceeded 40% under 1000 lux.[30] As discussed in the previous part, the desired PCE can be obtained by spectrum matching and non-radiative recombination suppression.

In this section, we overview the development of perovskite cells for indoor applications. As shown in Fig. 3, the bandgap engineering strategy can effectively match the absorption spectrum of perovskite with the emission spectrum of indoor light, and the film and interface engineering can concisely tailor the perovskite crystallization, retard the nonradiative recombination and promote carrier transport of devices. Moreover, further exploration of the potential applications of perovskite IPVs is also summarized, which includes large-area and flexible perovskite cells and integrated devices powered by perovskite cells.

Bandgap engineering of perovskites

Based on the emission spectra of the indoor light sources, the ideal bandgap for the perovskite was calculated to be 1.82–1.96 eV.[40,52] However, the optimal E_g value of popular perovskite is about 1.55 eV under AM 1.5G condition.[24] Hence, it is vital to broaden the perovskite bandgap to efficiently utilize the photons generated from the indoor light source. Take MAPbI$_3$ perovskite as an example, the electronic band structure mainly originates from the Pb 6s orbital and I 5p orbital.[53] Thus, the strategy of halide anion exchanging can effectively generate wider bandgap perovskites by varying the band edge states (Fig. 4a and b).[53–56] Lim *et al.* conducted concise control for the concentration of Br (Br = 0 to 30%) in MAPbI$_3$ perovskite.[57] As shown in Fig. 4c, the bandgap for the Br content increases linearly from 1.57 eV to 1.73 eV, with the Br content rising from 0% to 30%, and the devices with 10% ratio of Br exhibi-
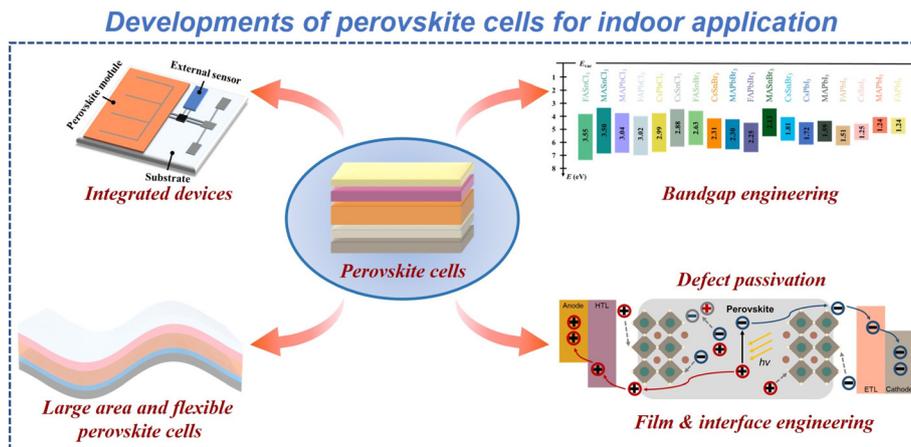
Fig. 3 Schematic diagram of the development of perovskite cells for indoor applications.
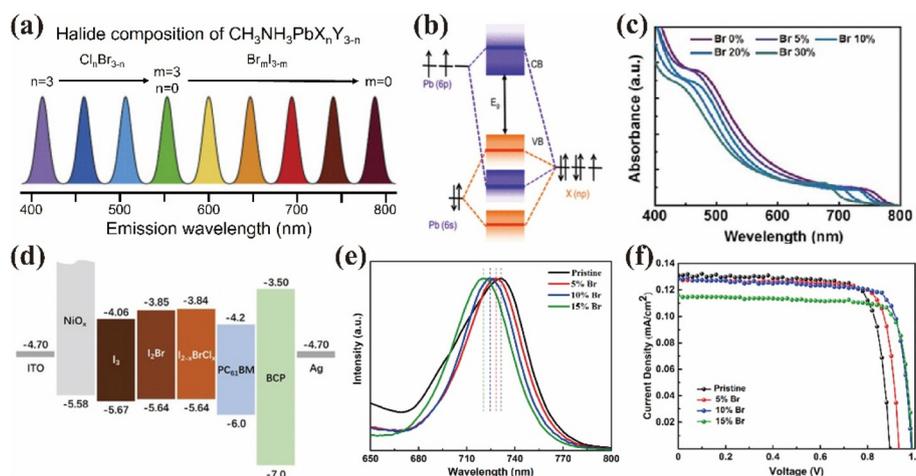

Fig. 4 (a) Emission-wavelength tunability of $CH_3NH_3PbX_nY_{3-n}$. Reproduced with permission from ref. 53. Copyright 2016, Springer Nature. (b) Schematic of the bonding/antibonding orbitals of $APbX_3$ perovskite, exhibiting the formation of valence band and conduction band. Reproduced with permission from ref. 55. Copyright 2016, American Chemical Society. (c) UV−vis absorption spectrum of $MAPbI_{3-x}Br_x$ films. Reproduced with permission from ref. 57. Copyright 2020, Elsevier Ltd. (d) Energy diagram of perovskite $MAPbI_3$, $MAPbI_2Br$, and $MAPbI_{2-x}BrCl_x$ cells. Reproduced with permission from ref. 58. Copyright 2019, WILEY-VCH. (e) Photoluminescence (PL) spectra of $CsPb(I_{1-x}Br_x)_3$ films. (f) J−V curves of the device with different Br concentrations under 1000 lux FL illumination. Reproduced with permission from ref. 62. Copyright 2022, American Chemical Society.

ted the best performance (34.5%). However, the mixed halide perovskite undergoes serious phase segregation when subjected to visible light, which undermines the long work stability of perovskite cells.[58] To prevent phase segregation, Cheng *et al.* further introduced Cl into mixed I/Br halide perovskite (Fig. 4d).[58] The involvement of Cl would cause shrinkage of the crystal lattice, which can effectively retard the anion migration and enhance the Pb–I and Pb–Br binding energy, leading to restrained segregation and improved stability. Hence, the triple anion perovskite cells exhibited good indoor efficiency and long-term working stability.

It has been reported that the cation substitution can also tailor the perovskite bandgap *via* the octahedral unit tilting.[8,59] Based on the calculated optimal E_g value of perovskites under indoor light illumination, Li *et al.* tailored the perovskite com-

position to modify the bandgap of perovskite.[60] The incorporation of Cs and Br could increase the E_g value to be around 1.77 eV, *i.e.*, $FA_{0.8}Cs_{0.2}Pb(I_{0.6}Br_{0.4})_3$, which enhanced the device performance under weak indoor light. Furthermore, the complete substitution of organic cations (MA^+ or FA^+) by inorganic cation Cs^+ can easily widen the perovskite bandgap, which can tune the bandgap range from 1.73 eV ($CsPbI_3$) to 2.3 eV ($CsPbBr_3$).[61] Considering the weak phase stability of photoactive α-phase $CsPbI_3$, Wang *et al.* introduced Br^- to effectively stabilize the Cs-based perovskite phase and further optimized the perovskite bandgap, which significantly enhanced the device performance under fluorescent lamp and white LED illumination (Fig. 4e and f).[62]

Though the ideal bandgap of perovskite can be tailored by the composition exchange, the corresponding devices are

reluctant to achieve comparable PCE based on the SQ theory, which is restricted by the fabrication of films with smooth and pinhole-free morphology and superior carrier transport. To this end, investigating new perovskite materials may pave a feasible way to overcome this obscure.

Film engineering of perovskites

The intensity of the indoor light source is three orders of magnitude lower than that of AM 1.5G, thus leading to a lower concentration of photogenerated carriers, where a higher concentration of carriers are trapped relative to photogenerated carrier ratios.[63–65] In addition, it has been reported that abundant defects are formed due to the rapid crystal growth from the solution process of perovskite films, which may cause notorious nonradiative recombination and thus lower the device performance (Fig. 5a).[66–68] Hence, the film engineering of perovskites can be an ideal strategy to suppress the defect-induced carrier recombination and further enhance the device performance.

Composition engineering has been conducted to tailor the perovskite crystallization process and passivate bulk defects of perovskite films. Dong *et al.* modulated the perovskite precursor composition to slow the nucleation of the perovskite, and thus formed a large–grain size and pinhole-free perovskite film by subtly replacing I^- in the lead source with $C_2O_4^{2-}$.[69] As shown in Fig. 5b, the modified perovskite film showed fewer defects and higher carrier mobility, allowing a high indoor PCE of 34.86% under 1000 lux of the corresponding device. Similarly, the changed cation source can also improve the perovskite film quality.[70] For the inorganic perovskite, the Cs precursor was changed from CsBr to cesium formate (CsFa), in which complex $HCOO \cdot Pb^+$ and $HCOO \cdot Cs^+$ formed. The perovskite crystallization was tailored by the volatilization of HCOOH in the annealing process, which induced the larger grain size and smoother surface of the perovskite film. Hence, the CsFa-doped perovskite cells showed enhanced performance under one sun and white LED illumination.

Apart from the composition substitution, the incorporation of additives can also improve the film quality and device characteristics. The additives can be categorized into few types such as Lewis base/acid, low-dimensional perovskites, ammonium salts and ionic liquids.[71–73] For example, Yang *et al.* introduced a Lewis base material, *N*,*N*′-bis(dimethylaminopropyl-*N*′′′-oxide)-perylene-3,4,9,10-tetracarboxidiimide (PDINO), into the precursor solution.[74] Owing to the great photoelectric characteristics of PDINO and the strong interaction between carbonyl groups in PDINO with the uncoordinated Pb atom in perovskites, the perovskite crystallinity and exciton separation ability were enhanced, inducing the improvement of indoor performance (Fig. 5c and d). Likewise,
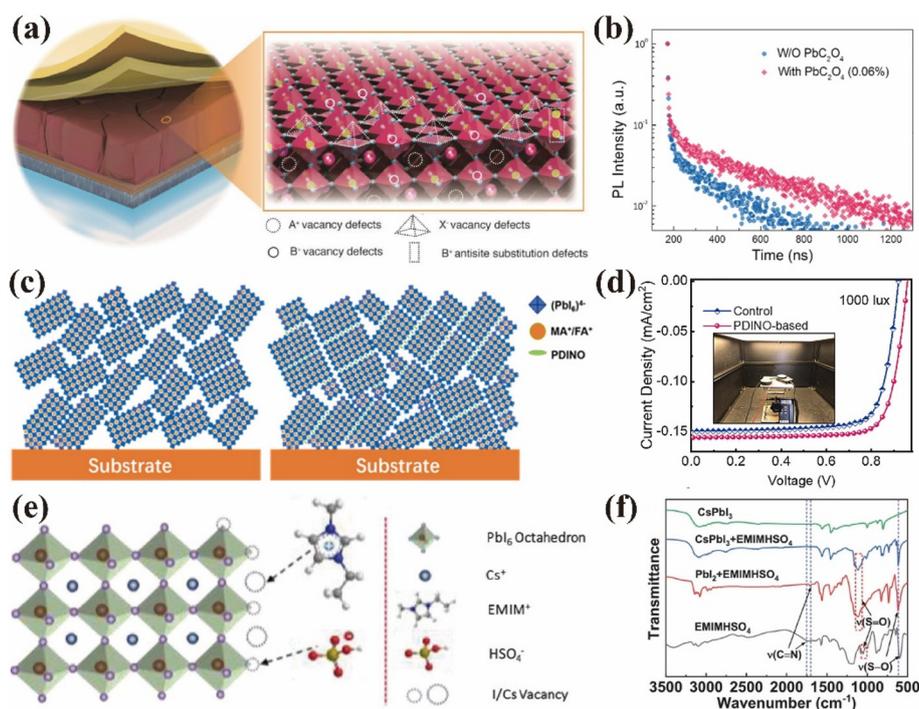
Fig. 5 (a) Schematic illustration of typical perovskite cells and detailed view of possible surface defects such as interstitials, substitutional and vacancies on perovskite crystals. Reproduced with permission from ref. 66. Copyright 2019, WILEY-VCH. (b) Time-resolved PL spectra for pristine and PbC_2O_4-doped perovskite films. Reproduced with permission from ref. 69. Copyright 2020, American Chemical Society. (c) Model diagram of the crystal alignment with/without PDINO. (d) *J*−*V* properties of the champion perovskite cells with/without PDINO obtained in indoor environments. Inset is the picture of the testing surroundings. Reproduced with permission from ref. 74. Copyright 2021, Elsevier Ltd. (e) Schematic illustration of defect passivation enabled by $EMIMHSO_4$. (f) Fourier-transform infrared spectra of $EMIMHSO_4$, PbI_2−$EMIMHSO_4$, $CsPbI_3$−$EMIMHSO_4$, and $CsPbI_3$ films. Reproduced with permission from ref. 73. Copyright 2022, WILEY-VCH.

the Lewis base phthalimide (2-N) molecules were added into the anti-solvent to modulate the crystallization process of $CsPbI_3$ films.[75] Based on the strong connection between 2-N and solvents, the author accurately controlled the evaporation of the solvent, and thus it facilitated prolonging the processing window and retard the crystal growth process. Hence, the modified device showed 40.07% PCE under 1062 lux illumination.

Moreover, a novel additive ionic liquid, 1-ethyl-3-methyl-imidazolium hydrogen sulfate ($EMIMHSO_4$), was introduced into perovskites.[73] As shown in Fig. 5e and f, this molecule showed strong interaction with the perovskite octahedral, where HSO_4^- exhibited a strong ability to withdraw electrons to eliminate the formation of donor defect V_I. In addition, the modified films presented a prolonged crystallization process owing to the strong interaction between perovskites and $EMIMHSO_4$, which caused a larger barrier to the perovskite growth. Hence, the modified devices exhibited a PCE of 37.24% under 1000 lux. In addition, Wang et al. reported the introduction of $(NH_4)_2C_2O_4 \cdot H_2O$ to treat $CsPbBrI_2$ perovskite films.[76] Particularly, $(NH_4)_2C_2O_4 \cdot H_2O$ decomposed into NH_3 and $H_2C_2O_4$ under high-temperature annealing, while NH_3 rapidly volatilized and the existence of $H_2C_2O_4$ tended to adjust the growth environment of perovskite grains, resulting in the secondary grain growth of perovskite films. Thus, the modified films exhibited a longer carrier lifetime and a lower trap density. As a result, the devices with $(NH_4)_2C_2O_4 \cdot H_2O$

additives showed promising performance (28.48%) under indoor light illumination.

Various additives have been incorporated into perovskite films to passivate the bulk defects and thus facilitate the effective transport of carriers.[77–79] However, these investigations are more based on the theory originating from standard sunlight, and few research studies focus on the carrier dynamic mechanisms of devices under indoor light illumination. Hence, to shed light on new mechanisms and establish new theories for perovskite IPVs, further investigations and analytical techniques are highly needed.

Interface engineering of devices

For perovskite cells, photogenerated carriers in the perovskite are extracted by the neighboring transport layer, and the collected charges are transferred to the external circuit via the electrode (Fig. 6a).[80] Thus, it is crucial to control the carrier dynamic concisely to achieve high indoor performance. To avoid the nonideal recombination of carriers, apart from the bulk defect modification of perovskite films, interface engineering has been proposed to eliminate the interfacial carrier nonradiative recombination and further improve the indoor PCE of perovskite cells.[81–83]

As for interface engineering, materials such as alkali metal compounds, organic molecules and conductive polymers, self-assembled monolayers, graphenes and graphene oxide derivatives were incorporated into the device interface to enhance
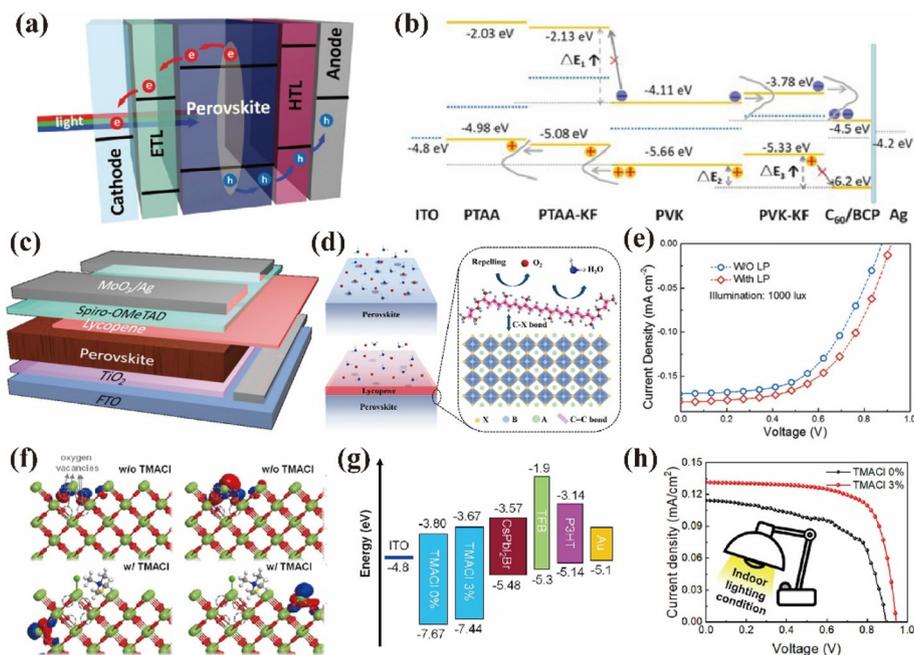
Fig. 6 (a) Schematic illustration of the carrier transport from the perovskite active layer of devices. Reproduced with permission from ref. 80. Copyright 2019, WILEY-VCH. (b) Energy level alignment of the perovskite cells. Reproduced with permission from ref. 87. Copyright 2020, Elsevier Ltd. (c) Schematic illustration of perovskite cells with the inserted LP thin film. (d) Mechanism diagram of the LP protection. (e) Indoor J–V curves for devices with/without LP layer. Reproduced with permission from ref. 31. Copyright 2021, WILEY-VCH. (f) Iso-surface plots of the highest occupied valence band (left) and the lowest occupied conduction band (right) of SnO_2 (110) with oxygen vacancies. (g) Energy level diagram of the device. (h) J–V curves of the unencapsulated devices. Reproduced with permission from ref. 89. Copyright 2021, American Chemical Society.

indoor performance.[84–86] For example, the ultrathin alkali halide was incorporated into the interface of the charge transport layer and perovskite layer to form a compact buffer layer, which can efficiently suppress the trap state and prevent ion migration.[87] Hence, the KF-modified devices showed improved indoor performance (Fig. 6b). Meanwhile, Cao *et al.* developed a strategy of buried interface modification by introducing KSCN as an interlayer into tin-based perovskite cells.[48] The incorporation of KSCN exhibited multiple improvements for the perovskite films and devices, such as optimizing energy bands, enhancing perovskite crystallization, reducing trap density and facilitating carrier transport. Based on the superior modification effect of KSCN, the devices showed a PCE of 17.57% under 1062 lux illumination, which is the highest indoor efficiency for tin-based perovskite cells. Moreover, phenethyl ammonium halides (PEAX, X = I, Br, and Cl) and their derivatives were introduced into the interface between the perovskite layer and the hole transport layer (HTL), which can effectively Polish the surface of perovskite film and passivate the surface defect, facilitating the carrier transport.[30,37,49] Thus, He *et al.* fabricated a device with a CH₃O–PEABr interlayer, achieving the record efficiency of 40.1% under 824.5 lux LED illumination.[30] Besides this, the organic long-chain molecule lycopene (LP) was introduced into the devices, which enabled perovskite films to present not only an enhanced average lifetime but also a decreased defect density owing to the C–X bond between perovskites and LP (Fig. 6c and d).[31] As a result, the LP-coated devices achieved an indoor efficiency of 40.24% at 1000 lux, which is the highest reported PCE in the literature (Fig. 6e).

To further optimize the energy level alignment of the device and lower the intrinsic defect of the transport layer, it is critical to regulate the transport layer. Noh *et al.* reported a bilayer structure of electron transport layer (ETL) by inserting a ZnO layer between ITO and SnO_2.[88] Herein, they effectively optimized the energy levels and improved the electron transport ability. The control of the annealing process of ZnO helped decrease the trap density and retard the charge recombination of the device, which, in turn, improved the device indoor PCE. In addition, tetramethylammonium chloride (TMACl) was also used to modify the SnO_2 ETL.[89] As shown in Fig. 6f and g, the incorporation of TMACl can not only passivate the oxygen vacancies of the SnO_2 surface by forming C–N–Sn bonds, but also upshift the energy level of SnO_2, which improved the electron transport in the $CsPbI_2Br$-based devices. As a result, the modified devices showed the optimized PCE under indoor conditions (Fig. 6h). Apart from the optimization of ETL, the HTL modification was also investigated. The incorporation of nicotinamide into PEDOT:PSS shifted down the work function of the HTL, contributing to a better energy level matching of the device and a smoother morphology.[90] Thus, the tin-based devices with nicotinamide showed a PCE of 17.26% under 1000 lux illumination. Li *et al.* incorporated poly(3-hexylthiophene) (P3HT) into PTAA, which effectively passivated the interface deep-level defects between the HTL and the perovskite film, owing to the coordination bond between the S atom in P3HT and uncoordinated Pb^{2+}, and thus promoted the hole carrier extraction.[91] Furthermore, the P3HT-doped HTL decreases the perovskite nucleus density, which is beneficial for preparing $MAPbI_3$ films with large grain sizes. With the incorporation of P3HT, the devices reached an indoor efficiency of 39.2% under 1000 lux.

The investigation of device carrier dynamic not only includes carrier separation and transport in the bulk film, but also contains the carrier extraction and transfer in the interface and transport layer. To further improve the indoor efficiency of devices, it is vital to understand how the interface allows more efficient carrier transport under indoor light illumination.

### Large area and flexible perovskite cells

In recent years, most of the reports on perovskite IPVs are based on small-area (<1 cm²) devices. However, to obtain higher P_{out} under low indoor light to drive low-power devices, it is necessary to conduct more extensive exploration on the large area up to module (>10 cm²) devices.

Till date, wide-bandgap perovskites are the prevailing candidates for indoor modules. Wu *et al.* prepared perovskite cells with a wider bandgap by adding Br ions into perovskite films to improve the E_g value. Under indoor FL irradiation, the large-area (4 cm²) devices prepared with 15% Br exhibited a PCE of 17.89%.[92] Based on $Cs_{0.05}(FA_{0.6}Ma_{0.4})_{0.95}Pb(I_{0.6}Br_{0.4})_3$ films, an appropriate amount of PEAI (2 mg mL⁻¹) was conformally post imposed on perovskite films, which improved the crystallinity and absorption of the film. Under the irradiation of halogen lamps with different illumination, the perovskite modules (4 sub cells in parallel, each sub-cell area: 20 cm²) can achieve the maximum power of 223 μW (at 200 lux), 510 μW (at 400 lux), 1023 μW (at 800 lux) and 1273 μW (at 1000 lux).[93] Currently, the efficiency for large-area perovskite cells has reached 36.36% (active area: 12.8 cm²), which is the highest efficiency reported for wide-bandgap perovskite cells to our knowledge.[94]

Meanwhile, minimizing the ohmic loss was employed to boost the large-area device efficiency. Bi *et al.* reported a hexafluorobenzene-assisted one-step blade-coating method (Fig. 7a) for the preparation of high-quality perovskite films with low ohmic loss.[95] With the modified perovskite film, the 1 cm² devices exhibited the PCE of 30.0% (100 lux) and 33.8% (1000 lux). Furthermore, the author successfully fabricated a self-powered drive LED indicator under indoor condition by connecting four sub-cells (each with an active area of 1 cm²) in series.

Combined with bandgap optimization and surface modification, it is urgent to further explore large-area perovskite film forming processes including optimization and matching of a blade-coating method, slot-die coating, inkjet printing, and screen printing. Impressively, Baker *et al.* achieved efficiencies of 11% (200 lux) and 18% (1000 lux) on a large A4-sized conductive glass substrate by a screen-printed perovskite module under FL illumination (Fig. 7b).[96] Nevertheless, there is little research on the large-area or module devices.

In order to meet the device requirements of lightweight and good performance, flexible perovskite cells have attracted wide-
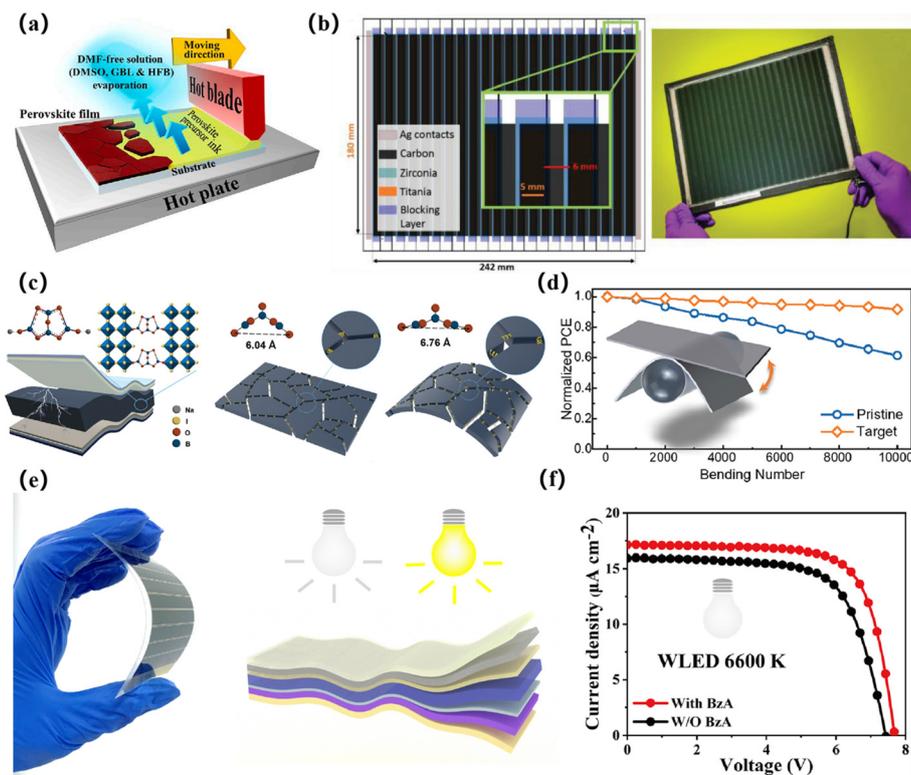
Fig. 7 (a) Schematic diagram of the one-step blade-coating method. Reproduced with permission from ref. 95. Copyright 2022, Elsevier Ltd. (b) Cross-section schematics and photos of adjacent cells in the module. Reproduced with permission from ref. 96. Copyright 2018, WILEY-VCH. (c) Schematic diagram of the device structure and the enlarged schematic of the structure of borax and interaction between borax and perovskites at grain boundaries; schematic diagram before and after bending of the flexible films with different shrinkage and stretch forms of borax-like spring. (d) Indoor PCE decay curves under different bending and different bending times of the pristine and target flexible devices. Reproduced with permission from ref. 98. Copyright 2022, WILEY-VCH. (e) Photographs and schematic diagram of the flexible perovskite module under indoor light illumination. (f) *J–V* curve of flexible devices with/without BzA seal mesh under WLED (1000 lux) illumination. Reproduced with permission from ref. 99. Copyright 2022, WILEY-VCH.

spread attention.[77] In 2020, Castro-Hermosa *et al.* reported indoor power generation by flexible devices made on flexible glass (FG) substrates with notable transmittance (>80%), sheet resistance (13 Ω per square) and superior mechanical stability (sheet resistance remains constant over 1600 bending procedures; curvature radius: 20.5 mm).[97] In addition, the perovskite cells based on FG achieved the PCE of 20.6% (16.7 μW cm^{-2}) and 22.6% (35.0 μW cm^{-2}) under 200 and 400 lux LED illumination, respectively. Apart from the research for the mechanical stability of substrates, the mechanical flexibility and environmental stability of perovskite films are the urgent challenges to be resolved. In 2022, Chen *et al.* proposed a three-dimensional borax crosslinking agent to fill the grain boundaries of perovskite films, initially achieving the stress release of three-dimensional spatial (Fig. 7c).[98] It is further confirmed that the mechanical and phase stability of the modified perovskite films were significantly improved. Based on this strategy, the PCE of flexible perovskite cells reached 31.85%, which is the highest reported record for flexible perovskite devices. The same year, the internal packing strategy was proposed by our team, where the cross-linking molecule benzyl acrylate (BzA) was introduced into the devices, which

can efficiently passivate defects at the grain boundaries.[99] Moreover, the crosslinking polymer molecular interlayer acted as a sealed mesh to protect against water, oxygen erosion and lead leakage from the devices. Interestingly, we validated the outstanding performance of flexible modules (24 cm^2, 30.73% under white LED, 26.48% under yellow LED) (Fig. 7d). Finally, Table 1 summarizes the photovoltaic characteristics of representative large-area and flexible perovskite cells in the past five years.[58,77,92,94,100]

Integrated devices with perovskite cells

In the high-speed development of manufacturing and internet communication technology, numerous smart products with low power consumption are fabricated and applied under indoor conditions, *e.g.*, homes, offices and factories for environment monitoring or digital information transfer.[2] To ensure the stable operation of IoT systems, it is vital to develop self-powered devices to replace traditional devices supplied by non-self-rechargeable batteries. In recent years, perovskite cells exhibit great application potential for self-powered devices in IoT systems, due to their superior characteristics such as high power supply, easy fabrication, low cost and good

Table 1 Summary of large area and flexible indoor perovskite cells

Substrate	Perovskite materials	Bandgap (eV)	Light source	PCE (%)	P_{out} (µW cm^{-2})	Area (cm^2)	Year	Ref.
Rigid	$MAPbI_3$	1.59	FL (100 lux)	11	3.03	198	2018	96
			(1000 lux)	18	50.51			
Rigid	$MA_{0.85}Cs_{0.15}Pb(I_{0.85}Br_{0.15})_3$	1.66	FL (600 lux)	17.35	34.01	4	2019	92
			(1000 lux)	17.89	58.1			
Rigid	$MAPbI_{2-x}BrCl_x$	1.797	FL (1000 lux)	30.6	84.36	2.25	2019	58
Rigid	$MAPbI_3$	1.59	WLED (100 lux)	30.0	—	1	2022	95
			(1000 lux)	33.8	—			
Rigid	$Cs_{0.17}FA_{0.83}PbI_{3-x}Br_x$	1.77	TL84 (1000 lux)	36.36	99.92	12.8	2022	94
Flexible	$MAPbI_3$	1.59	LED (200 lux)	20.6	16.7	0.1	2020	97
			(400 lux)	22.6	35.0			
Flexible	$MA_{0.05}FA_{0.95}Pb(I_{0.97}Br_{0.03})_3$	1.63	WLED (400 lux)	23.33	63	0.12	2020	77
			(1000 lux)	25.74	175			
Flexible	$Cs_{0.17}FA_{0.83}Pb(I_{0.7}Br_{0.3})_3$	1.72	WLED (200 lux)	30.0	22.9	0.1	2022	10
			(1000 lux)	30.9	121.8			
Flexible	$FAPbI_3$	1.55	LED (1062 lux)	31.85	106	0.07	2022	98
Flexible	$CsFAMAPbI_{3-x}Br_x$	1.53	LED (1000 lux)	30.73	95.3	24	2022	99
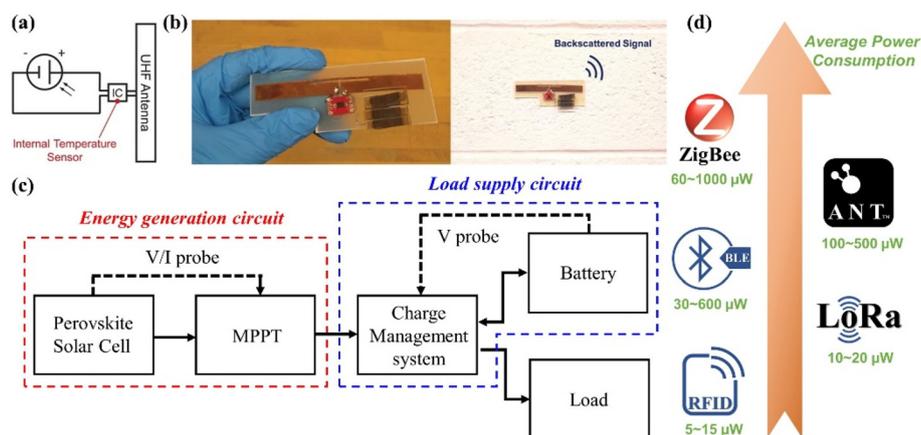
Fig. 8 (a) Circuit diagram of the prototype IPV-backscatter sensor. (b) Pictures of the IPV-backscatter sensor. Reproduced with permission from ref. 104. Copyright 2022, WILEY-VCH. (c) Proposed perovskite cell energy harvesting system. Reproduced with permission from ref. 105. Copyright 2022, MDPI. (d) Average power consumption of wireless protocols.

adaptability to different environments.[101–103] Extensive research has been conducted to explore the integrated manufacture of perovskite cell–based self-powered devices for indoor applications. For example, Mathews *et al.* fabricated self-powered sensors by integrating perovskite cells and a radiofrequency (RF)-backscatter temperature sensor.[104] Through the strategy of multiplication engineering and anion exchange, a wide-bandgap perovskite (1.84 eV) with excellent phase stability was fabricated. In addition, the corresponding devices showed a PCE of 18.5% under compact fluorescence. As shown in Fig. 8a and b, a module with three cells connected in series was integrated to provide charging voltages for the IoT nodes. This power supply device enhanced the backscatter communication range of the sensor up to 7.2 times, reaching a maximum of 5.1 m while maintaining a measurement period of 1.24 s. Similarly, the energy harvesting system, which consisted of perovskite cells, an energy harvesting circuitry, and a load management system, was developed for the IoT application (Fig. 8c).[105] The 3 series 2 parallel connected devices

with an area of 2.25 cm^2 were used to deliver the energy. Perovskite cell generation can efficiently power the load in the sleep mode under 1000 lux indoor light illumination, and excess power was stored by the battery for the probe period. Moreover, as shown in Fig. 8d, newly developed wireless protocols such as ZigBee, ANT, BLE, LoRA backscatter and RFID exhibit a lower average power consumption, in the range of 5 µW to 1000 µW, than that of traditional protocols (*e.g.*, Wi–Fi or SigFox).[2] Meanwhile, it can be estimated that a 10 cm^2 perovskite module with an efficiency over 35% under 300 µW cm^{-2} (1000 lux) WLED could produce a power of over 1 mW, which could efficiently suffice for the work consumption of these nodes.

Conclusions and perspectives

Owing to the rapid growth of the IoT market, the demand for self-powering supply is gradually increasing for the long-time

working stability of IoT systems. Meanwhile, IPVs, especially perovskite IPVs, can be good candidates for the power supply without external batteries. Considering the features of indoor condition, the spectrum match for the indoor light and perovskite materials is the key point for the good performance of devices. Moreover, the defect passivation for the bulk and interface cannot be ignored either. In this review, we summarized feasible strategies, including bandgap engineering, film engineering of perovskites and interface engineering of devices, which enhanced the performance of perovskite cells. Based on the cation or anion exchange, the perovskite with the ideal bandgap can be synthesized. Furthermore, the modulated perovskite crystallization and enhanced carrier transport in the device have been achieved by the incorporation of additives and interlayers. Although the indoor efficiency (over 40%) has far exceeded the outdoor efficiency of perovskite cells, their performance is still undesirable compared with the SQ efficiency limit (57%). Moreover, few research studies consider the carrier dynamics mechanism of perovskite cells under dimming light. Hence, we put forward the possible approaches shown as follows, which may accelerate the further improvement of the indoor performance of perovskite cells.

Ultrafast carrier dynamics mechanism about perovskite IPVs

Perovskite IPVs exhibit a unique phenomenon of "low-concentration photogenerated carriers" under low illumination. The unique non-uniform energy distribution of artificial light sources leads to the "excitation–relaxation" process of low-concentration photogenerated carriers being more sensitive to defects. The defects of perovskite cells are mainly concentrated in perovskite films, whose defect characteristics include defect types (vacancy defects, interstitial defects, and substitution defects), defect levels (shallow-level defects and deep-level defects) and defect distribution (body defects and surface defects). For indoor artificial light sources (low illuminance and non-uniform spectral distribution), which are greatly different from outdoor sunlight, the corresponding law between low-order SRH recombination dominated by carrier recombination and defect characteristics has not been resolved yet. As the origin of charge-carrier recombination, the dynamic mechanism of light capture, transport and related physical models still lacks deeper research and cognition. In recent years, basic studies by ultrafast spectroscopy have played an important role in revealing key issues such as light capture, charge generation, recombination and transport mechanisms. Therefore, for perovskite IPVs, the corresponding mechanism studied by ultrafast spectroscopy technology can uncover the ultrafast carrier dynamic process and relaxation mechanism under low indoor light illumination, where further research is expected to provide the theoretical basis for material development and device optimization.

New perovskite materials

Due to the peculiar spectrum of indoor light, the bandgap engineering of perovskites has been proposed as an ideal way to achieve the maximum absorption of photons. In addition,

most reports have focused on anion or cation exchanging in the three-dimensional (3D) perovskite for bandgap regulation, which may face the challenge of poor film quality, phase segregation or weak stability. Besides, the limited carrier lifetime, high trap density, slow carrier mobility and so on caused by the unsuitable exchanging of anions or cations strongly restrict the development of perovskite IPVs. However, the introduction of novel perovskite materials such as 2D perovskites, perovskite quantum dots (PQDs) and single-crystal perovskites could be the alternative solutions for the bandgap tuning. As for the 2D perovskites, their bandgap can be easily adjusted by changing the thickness of the metal–halide slab.[106] For example, the bandgap of $BA_2MA_{n-1}Pb_nI_{3n+1}$ decreases from 2.49 to 1.68 eV, while the number of layers increases from 1 to 5.[107] Importantly, they show good environmental stability due to the hydrophobic groups. Similarly, the PQDs show the tuneable bandgap owing to a quantum-confinement effect, *i.e.*, $CsPbI_3$ QDs (ranging from 1.82 to 2.07 eV with the QD size decreased from 12.5 to 3 nm).[108] Furthermore, the efficiency of PQD-based devices is expected to surpass the SQ limit by multiple exciton generation, turning to make use of hot carriers. Based on the low trap density and superior stability of single-crystal perovskites, it is feasible to fabricate high-quality absorption layer with a suitable bandgap, and thus achieve high efficiency under indoor light illumination.[109]

Long-term stability and Pb toxicity

Low indoor light intensity leads to the low concentration of photogenerated carriers of devices and low heat by working conditions, which enable the device to remain stable under indoor conditions. For the long-term stability of perovskite cells, the bulk perovskite stability and device encapsulation should be taken into consideration. As for the bulk perovskite stability, these feasible strategies mentioned in the main text can be conducted to strengthen the perovskite lattices. Besides this, the new perovskite materials can be the good candidates for the bulk perovskite stability. The device encapsulation such as cover encapsulation, film encapsulation and hybrid encapsulation can further protect the cells from the invasion of humidity and oxygen. However, most of the research studies focused on the encapsulation of rigid devices. To expand the application of perovskite IPVs, it is crucial to explore the flexible device encapsulation.

It has been reported that the density of $MAPbI_3$ is about 4.3 g cm^{-3}.[10] Thus, the Pb weight content with 500 nm film thickness can be estimated to be 2.15 g m^{-2}, which is far below the glass or flexible substrate weight content. The trace content is less than the set limit for the Pb content in electronics imposed by many countries (<0.1% weight). Nevertheless, to avoid the potential risks, the community would expect to further reduce or limit Pb issues in the practical products. To this end, proper physical encapsulation is essentially required. Moreover, chemical adsorption engineering can also inhibit the lead leakage by immobilizing with lead ions from degraded perovskites. Meanwhile, the develop-

ment of lead-free perovskite cells with good performance needs to be considered.

As discussed above, the further utilization of new advanced technologies and the introduction of superior perovskite materials may pave a facial way to deeply explore the mechanism of carrier transport under indoor light illumination and promote the efficiency improvement of perovskite cells. With the complement of theory and enhancement of performance, perovskite IPVs could play a crucial role in the stable power supply for IoT systems.

Conflicts of interest

There are no conflicts to declare.

Acknowledgements

References

1 B. Li, B. Hou and G. A. J. Amaratunga, *InfoMat*, 2021, **3**, 445–459.

2 I. Mathews, S. N. Kantareddy, T. Buonassisi and I. M. Peters, *Joule*, 2019, **3**, 1415–1426.

3 K. L. Wang, Y. H. Zhou, Y. H. Lou and Z. K. Wang, *Chem. Sci.*, 2021, **12**, 11936–11954.

4 V. Pecunia, L. G. Occhipinti and R. L. Z. Hoye, *Adv. Energy Mater.*, 2021, **11**, 2100698.

5 C. Polyzoidis, K. Rogdakis and E. Kymakis, *Adv. Energy Mater.*, 2021, **11**, 2101854.

6 X. Hou, Y. Wang, H. K. H. Lee, R. Datt, N. Uslar Miano, D. Yan, M. Li, F. Zhu, B. Hou, W. C. Tsoi and Z. Li, *J. Mater. Chem. A*, 2020, **8**, 21503–21525.

7 X. Liu and E. Sánchez-Sinencio, *IEEE Trans. Very Large Scale Integr. VLSI Syst.*, 2015, **23**, 3065–3075.

8 M. Li, F. Igbari, Z. K. Wang and L. S. Liao, *Adv. Energy Mater.*, 2020, **10**, 2000641.

9 S. Biswas and H. Kim, *Polymers*, 2020, **12**, 1338.

10 B. T. Muhammad, S. Kar, M. Stephen and W. L. Leong, *Mater. Today Energy*, 2022, **23**, 100907.

11 L. Portilla, K. Loganathan, H. Faber, A. Eid, J. G. D. Hester, M. M. Tentzeris, M. Fattori, E. Cantatore, C. Jiang, A. Nathan, G. Fiori, T. Ibn-Mohammed, T. D. Anthopoulos and V. Pecunia, *Nat. Electron.*, 2023, **6**, 10–17.

12 P. D. Antunez, D. M. Bishop, Y. Luo and R. Haight, *Nat. Energy*, 2017, **2**, 884–890.

13 E. Moon, D. Blaauw and J. D. Phillips, *IEEE Trans. Electron Devices*, 2017, **64**, 15–20.

14 H. Zheng, D. Li, C. Ran, Q. Zhong, L. Song, Y. Chen, P. Müller-Buschbaum and W. Huang, *Sol. RRL*, 2021, **5**, 2100042.

15 J. Xu, J. Xi, H. Dong, N. Ahn, Z. Zhu, J. Chen, P. Li, X. Zhu, J. Dai, Z. Hu, B. Jiao, X. Hou, J. Li and Z. Wu, *Nano Energy*, 2021, **88**, 106286.

16 Y. Peng, T. N. Huq, J. Mei, L. Portilla, R. A. Jagt, L. G. Occhipinti, J. L. MacManus-Driscoll, R. L. Z. Hoye and V. Pecunia, *Adv. Energy Mater.*, 2021, **11**, 2002761.

17 N. H. Reich, W. G. J. H. M. V. Sark, E. A. Alsema, R. W. Lof, R. E. I. Schropp, W. C. Sinke and W. C. Turkenburg, *Sol. Energy Mater. Sol. Cells*, 2009, **93**, 1471–1481.

18 M. Nishita, S.-Y. Park, T. Nishio, K. Kamizaki, Z. Wang, K. Tamada, T. Takumi, R. Hashimoto, H. Otani, G. J. Pazour, V. W. Hsu and Y. Minami, *Sci. Rep.*, 2017, **7**, 1.

19 I. Mathews, P. J. King, F. Stafford and R. Frizzell, *IEEE J. Photovoltaics*, 2016, **6**, 230–235.

20 A. S. Teran, E. Moon, W. Lim, G. Kim, I. Lee, D. Blaauw and J. D. Phillips, *IEEE Trans. Electron Devices*, 2016, **63**, 2820–2825.

21 Q. Li, K. Shen, R. Yang, Y. Zhao, S. Lu, R. Wang, J. Dong and D. Wang, *Sol. Energy*, 2017, **157**, 216–226.

22 L. Xie, W. Song, J. Ge, B. Tang, X. Zhang, T. Wu and Z. Ge, *Nano Energy*, 2021, **82**, 105770.

23 L. K. Jagadamma and S. Wang, *Front. Chem.*, 2021, **9**, 632021.

24 H. Opoku, J. Hyeon Lee, J. Won Shim and J. Woong Jo, *Chem. – Eur. J.*, 2022, **28**, e202200266.

25 M. L. Jiang, J.-J. Wen, Z.-M. Chen, W.-H. Tsai, T.-C. Lin, T. J. Chow and Y. J. Chang, *ChemSusChem*, 2019, **12**, 3654–3665.

26 K. Wojciechowski and D. Forgács, *ACS Energy Lett.*, 2022, **7**, 3729–3733.

27 J. Chen, Y. Yang, H. Dong, J. Li, X. Zhu, J. Xu, F. Pan, F. Yuan, J. Dai, B. Jiao, X. Hou, A. K.-Y. Jen and Z. Wu, *Sci. Adv.*, 2022, **8**, eabk2722.

28 A. K. Jena, A. Kulkarni and T. Miyasaka, *Chem. Rev.*, 2019, **119**, 3036–3103.

29 J. Y. Kim, J. W. Lee, H. S. Jung, H. Shin and N. G. Park, *Chem. Rev.*, 2020, **120**, 7867–7918.

30 X. He, J. Chen, X. Ren, L. Zhang, Y. Liu, J. Feng, J. Fang, K. Zhao and S. F. Liu, *Adv. Mater.*, 2021, **33**, e2100770.

31 C. Dong, X. M. Li, C. Ma, W. F. Yang, J. J. Cao, F. Igbari, Z. K. Wang and L. S. Liao, *Adv. Funct. Mater.*, 2021, **31**, 2011242.

32 Y. Cui, H. Yao, T. Zhang, L. Hong, B. Gao, K. Xian, J. Qin and J. Hou, *Adv. Mater.*, 2019, **31**, 1904512.

33 B. Parida, A. Singh, A. K. Kalathil Soopy, S. Sangaraju, M. Sundaray, S. Mishra, S. F. Liu and A. Najar, *Adv. Sci.*, 2022, **9**, e2200308.

34 Y. Wang, C. Duan, P. Lv, Z. Ku, J. Lu, F. Huang and Y. B. Cheng, *Natl. Sci. Rev.*, 2021, **8**, nwab075.

35 X. Dai, Y. Deng, C. H. Van Brackle, S. Chen, P. N. Rudd, X. Xiao, Y. Lin, B. Chen and J. Huang, *Adv. Energy Mater.*, 2019, **10**, 1903108.

36 Y. Lei, Y. Chen, R. Zhang, Y. Li, Q. Yan, S. Lee, Y. Yu, H. Tsai, W. Choi, K. Wang, Y. Luo, Y. Gu, X. Zheng, C. Wang, C. Wang, H. Hu, Y. Li, B. Qi, M. Lin, Z. Zhang, S. A. Dayeh, M. Pharr, D. P. Fenning, Y.-H. Lo, J. Luo, K. Yang, J. Yoo, W. Nie and S. Xu, *Nature*, 2020, **583**, 790–795.

37 M. Lee, E. Choi, A. M. Soufiani, J. Lim, M. Kim, D. Chen, M. A. Green, J. Seidel, S. Lim, J. Kim, X. Dai, R. Lee-Chin, B. Zheng, Z. Hameiri, J. Park, X. Hao and J. S. Yun, *Adv. Funct. Mater.*, 2021, **31**, 2008908.

38 A. Venkateswararao, J. K. W. Ho, S. K. So, S.-W. Liu and K.-T. Wong, *Mater. Sci. Eng., R*, 2020, **139**, 100517.

39 N. Yan, C. Zhao, S. You, Y. Zhang and W. Li, *Chin. Chem. Lett.*, 2020, **31**, 643–653.

40 J. K. W. Ho, H. Yin and S. K. So, *J. Mater. Chem. A*, 2020, **8**, 1717–1723.

41 H. Yin, J. K. W. Ho, S. H. Cheung, R. J. Yan, K. L. Chiu, X. Hao and S. K. So, *J. Mater. Chem. A*, 2018, **6**, 8579–8585.

42 I. Mathews, G. Kelly, P. J. King and R. Frizzell, *IEEE 40th Photovoltaics Spec. Conf. PVSC*, 2014, 0510–0513.

43 Y. Zhou, T. M. Khan, J. W. Shim, A. Dindar, C. Fuentes-Hernandez and B. Kippelen, *J. Mater. Chem. A*, 2014, **2**, 3492–3497.

44 J. Chen, H. Dong, J. Li, X. Zhu, J. Xu, F. Pan, R. Xu, J. Xi, B. Jiao, X. Hou, K. Wei Ng, S.-P. Wang and Z. Wu, *ACS Energy Lett.*, 2022, **7**, 3685–3694.

45 L. Li, Y. Wang, X. Wang, R. Lin, X. Luo, Z. Liu, K. Zhou, S. Xiong, Q. Bao, G. Chen, Y. Tian, Y. Deng, K. Xiao, J. Wu, M. I. Saidaminov, H. Lin, C.-Q. Ma, Z. Zhao, Y. Wu, L. Zhang and H. Tan, *Nat. Energy*, 2022, **7**, 708–717.

46 J. J. Yoo, S. S. Shin and J. Seo, *ACS Energy Lett.*, 2022, **7**, 2084–2091.

47 M. A. Green, E. D. Dunlop, J. Hohl-Ebinger, M. Yoshita, N. Kopidakis and X. Hao, *Prog. Photovoltaics Res. Appl.*, 2022, **30**, 3–12.

48 J.-J. Cao, Y.-H. Lou, W.-F. Yang, K.-L. Wang, Z.-H. Su, J. Chen, C.-H. Chen, C. Dong, X.-Y. Gao and Z.-K. Wang, *Chem. Eng. J.*, 2022, **433**, 133832.

49 Z. Li, J. Zhang, S. Wu, X. Deng, F. Li, D. Liu, C. C. Lee, F. Lin, D. Lei, C.-C. Chueh, Z. Zhu and A. K. Y. Jen, *Nano Energy*, 2020, **78**, 105377.

50 Y.-T. Lin, G. Kumar and F.-C. Chen, *Sol. Energy*, 2020, **211**, 822–830.

51 K. Kawata, K. Tamaki and M. Kawaraya, *J. Photopolym. Sci. Technol.*, 2015, **28**, 415–417.

52 M. Freunek, M. Freunek and L. M. Reindl, *IEEE J. Photovoltaics*, 2013, **3**, 59–64.

53 V. K. Ravi, G. B. Markad and A. Nag, *ACS Energy Lett.*, 2016, **1**, 665–671.

54 B. R. Sutherland and E. H. Sargent, *Nat. Photonics*, 2016, **10**, 295–302.

55 M. J. Wu, C. C. Kuo, L. S. Jhuang, P. H. Chen, Y. F. Lai and F. C. Chen, *Adv. Energy Mater.*, 2019, **9**, 665–671.

56 T. C. Yang, P. Fiala, Q. Jeangrous and C. Ballif, *Joule*, 2018, **2**, 1421–1436.

57 J. W. Lim, H. Kwon, S. H. Kim, Y.-J. You, J. S. Goo, D.-H. Ko, H. J. Lee, D. Kim, I. Chung, T. G. Kim, D. H. Kim and J. W. Shim, *Nano Energy*, 2020, **75**, 104984.

58 R. Cheng, C.-C. Chung, H. Zhang, F. Liu, W.-T. Wang, Z. Zhou, S. Wang, A. B. Djurišić and S.-P. Feng, *Adv. Energy Mater.*, 2019, **9**, 1901980.

59 T. A. S. Doherty, S. Nagane, D. J. Kubicki, Y. Jung, D. N. Johnstone, A. N. Iqbal, D. Guo, K. Frohna, M. Danaie, E. M. Tennyson, S. Macpherson, A. Abfalterer, M. Anaya, Y. Chiang, P. Crout, F. S. Ruggeri, S. Collins, C. P. Grey, A. Walsh, P. A. Midgley and S. D. Stranks, *Science*, 2021, **374**, 1598–1605.

60 Y. Li, R. Li and Q. Lin, *Small*, 2022, **18**, e2202028.

61 J. Tian, Q. Xue, Q. Yao, N. Li, C. J. Brabec and H. L. Yip, *Adv. Energy Mater.*, 2020, **10**, 2000183.

62 M. Wang, Q. Wang, J. Zhao, Y. Xu, H. Wang, X. Zhou, S. Yang, Z. Ci and Z. Jin, *ACS Appl. Mater. Interfaces*, 2022, **14**, 11528–11537.

63 T. Supasai, K. T. Soe, T. Smerchit, F. Azad, N. Thongprong, N. Kayunkid, I. M. Tang, P. Kumnorkaew, A. Kaewprajak, V. Tangwarodomnukun, Y. Li, S. Chanyawadee, J. Yuan and N. Rujisamphan, *Adv. Energy Sustainability Res.*, 2021, **3**, 2100143.

64 G. Lucarelli, F. Di Giacomo, V. Zardetto, M. Creatore and T. M. Brown, *Nano Res.*, 2017, **10**, 2130–2145.

65 P. Ghosh, J. Bruckbauer, C. Trager-Cowan and L. Krishnan Jagadamma, *Appl. Surf. Sci.*, 2022, **592**, 152865.

66 E. Aydin, M. De Bastiani and S. De Wolf, *Adv. Mater.*, 2019, **31**, e1900428.

67 K. S. Kim, I. S. Jin, S. H. Park, S. J. Lim and J. W. Jung, *ACS Appl. Mater. Interfaces*, 2020, **12**, 36228–36236.

68 J. Kim, J. H. Jang, E. Choi, S. J. Shin, J.-H. Kim, G. G. Jeon, M. Lee, J. Seidel, J. H. Kim, J. S. Yun and N. Park, *Cell Rep. Phys. Sci.*, 2020, **1**, 100273.

69 C. Dong, M. Li, Y. Zhang, K. L. Wang, S. Yuan, F. Igbari, Y. Yang, X. Gao, Z. K. Wang and L. S. Liao, *ACS Appl. Mater. Interfaces*, 2020, **12**, 836–843.

70 Q. Guo, Y. Ding, Z. Dai, Z. Chen, M. Du, Z. Wang, L. Gao, C. Duan, Q. Guo and E. Zhou, *Phys. Chem. Chem. Phys.*, 2022, **24**, 17526–17534.

71 X. Cao, J. Li, H. Dong, P. Li, Q. Fan, R. Xu, H. Li, G. Zhou and Z. Wu, *Adv. Funct. Mater.*, 2021, **31**, 2104344.

72 Y. Zhao, F. Ma, Z. Qu, S. Yu, T. Shen, H.-X. Deng, X. Chu, X. Peng, Y. Yuan, X. Zhang and J. You, *Science*, 2022, **377**, 531–534.

73 Y. Du, Q. Tian, X. Chang, J. Fang, X. Gu, X. He, X. Ren, K. Zhao and S. F. Liu, *Adv. Mater.*, 2022, **34**, e2106750.

74 F. Yang, Z. Su, J. Pascual, M. Li, H. Liu, C. Qin, X. Gao, G. Li, Z. Li and Z. Wang, *J. Power Sources*, 2022, **520**, 230785.

75 K. L. Wang, Z. H. Su, Y. H. Lou, Q. Lv, J. Chen, Y. R. Shi, C. H. Chen, Y. H. Zhou, X. Y. Gao, Z. K. Wang and L. S. Liao, *Adv. Energy Mater.*, 2022, **12**, 2201274.

76 K.-L. Wang, X.-M. Li, Y.-H. Lou, M. Li and Z.-K. Wang, *Sci. Bull.*, 2021, **66**, 347–353.

77 S. Kim, H. Oh, G. Kang, I. K. Han, I. Jeong and M. Park, *ACS Appl. Energy Mater.*, 2020, **3**, 6995–7003.

78 C. H. Chen, Y. H. Lou, K. L. Wang, Z. H. Su, C. Dong, J. Chen, Y. R. Shi, X. Y. Gao and Z. K. Wang, *Adv. Energy Mater.*, 2021, **11**, 2101538.

79 C. Dong, J. Chen, C.-H. Chen, Y.-R. Shi, W.-F. Yang, K.-L. Wang, Z.-K. Wang and L.-S. Liao, *Nano Energy*, 2022, **94**, 106866.

80 T. H. Han, S. Tan, J. Xue, L. Meng, J. W. Lee and Y. Yang, *Adv. Mater.*, 2019, **31**, e1803515.

81 Z. W. Gao, Y. Wang and W. C. H. Choy, *Adv. Energy Mater.*, 2022, **12**, 2104030.

82 G. Alosaimi, S. J. Shin, R. L. Chin, J. H. Kim, J. S. Yun and J. Seidel, *Adv. Energy Mater.*, 2021, **11**, 2101739.

83 W. Dong, W. Qiao, S. Xiong, J. Yang, X. Wang, L. Ding, Y. Yao and Q. Bao, *Nano-Micro Lett.*, 2022, **14**, 108.

84 S. Bi, X. Leng, Y. Li, Z. Zheng, X. Zhang, Y. Zhang and H. Zhou, *Adv. Mater.*, 2019, **31**, 1805708.

85 J. Zhuang, P. Mao, Y. Luan, X. Yi, Z. Tu, Y. Zhang, Y. Yi, Y. Wei, N. Chen, T. Lin, F. Wang, C. Li and J. Wang, *ACS Energy Lett.*, 2019, **4**, 2913–2921.

86 J. Chen and N.-G. Park, *ACS Energy Lett.*, 2020, **5**, 2742–2786.

87 J. Xu, H. Dong, J. Xi, Y. Yang, Y. Yu, L. Ma, J. Chen, B. Jiao, X. Hou, J. Li and Z. Wu, *Nano Energy*, 2020, **75**, 104940.

88 Y. W. Noh, I. S. Jin, K. S. Kim, S. H. Park and J. W. Jung, *J. Mater. Chem. A*, 2020, **8**, 17163–17173.

89 B. Parida, I. S. Jin and J. W. Jung, *Chem. Mater.*, 2021, **33**, 5850–5858.

90 W.-F. Yang, J.-J. Cao, J. Chen, K.-L. Wang, C. Dong, Z.-K. Wang and L.-S. Liao, *Sol. RRL*, 2021, **5**, 2100713.

91 N. Li, A. Feng, X. Guo, J. Wu, S. Xie, Q. Lin, X. Jiang, Y. Liu, Z. Chen and X. Tao, *Adv. Energy Mater.*, 2021, **12**, 2103241.

92 M.-J. Wu, C.-C. Kuo, L.-S. Jhuang, P.-H. Chen, Y.-F. Lai and F.-C. Chen, *Adv. Energy Mater.*, 2019, **9**, 1901863.

93 M. Lee, E. Choi, A. M. Soufiani, J. Lim, M. Kim, D. Chen, M. A. Green, J. Seidel, S. Lim, J. Kim, X. Dai, R. Lee-Chin, B. Zheng, Z. Hameiri, J. Park, X. Hao and J. S. Yun, *Adv. Funct. Mater.*, 2021, **31**, 2008908.

94 C. Zhang, C. Liu, Y. Gao, S. Zhu, F. Chen, B. Huang, Y. Xie, Y. Liu, M. Ma, Z. Wang, S. Wu, R. E. I. Schropp and Y. Mai, *Adv. Sci.*, 2022, **9**, 2204138.

95 Z. Bi, X. Xu, X. Chen, Y. Zhu, C. Liu, H. Yu, Y. Zheng, P. A. Troshin, A. Guerrero and G. Xu, *Chem. Eng. J.*, 2022, **446**, 137164.

96 F. De Rossi, J. A. Baker, D. Beynon, K. E. A. Hooper, S. M. P. Meroni, D. Williams, Z. Wei, A. Yasin, C. Charbonneau, E. H. Jewell and T. M. Watson, *Adv. Mater. Technol.*, 2018, **3**, 1800156.

97 S. Castro-Hermosa, G. Lucarelli, M. Top, M. Fahland, J. Fahlteich and T. M. Brown, *Cell Rep. Phys. Sci.*, 2020, **1**, 100045.

98 C.-H. Chen, Z.-H. Su, Y.-H. Lou, Y.-J. Yu, K.-L. Wang, G.-L. Liu, Y.-R. Shi, J. Chen, J.-J. Cao, L. Zhang, X.-Y. Gao and Z.-K. Wang, *Adv. Mater.*, 2022, **34**, 2200320.

99 X. Zhu, H. Dong, J. Chen, J. Xu, Z. Li, F. Yuan, J. Dai, B. Jiao, X. Hou, J. Xi and Z. Wu, *Adv. Funct. Mater.*, 2022, **32**, 2202408.

100 C. Teixeira, P. Spinelli, L. A. Castriotta, D. Müller, S. Öz, L. Andrade, A. Mendes, A. D. Carlo, U. Würfel, K. Wojciechowski and D. Forgács, *Adv. Funct. Mater.*, 2022, **32**, 2206761.

101 M. Seri, F. Mercuri, G. Ruani, Y. Feng, M. Li, Z.-X. Xu and M. Muccini, *Energy Technol.*, 2021, **9**, 2000901.

102 S. Sahare, H. D. Pham, D. Angmo, P. Ghoderao, J. MacLeod, S. B. Khan, S. L. Lee, S. P. Singh and P. Sonar, *Adv. Energy Mater.*, 2021, **11**, 2101085.

103 G. Tang and F. Yan, *Nano Today*, 2021, **39**, 101155.

104 I. Mathews, S. N. R. Kantareddy, S. Sun, M. Layurova, J. Thapa, J.-P. Correa-Baena, R. Bhattacharyya, T. Buonassisi, S. Sarma and I. M. Peters, *Adv. Funct. Mater.*, 2019, **29**, 1904072.

105 Y. Olzhabay, A. Ng and I. A. Ukaegbu, *Energies*, 2021, **14**, 7946.

106 G. Wu, R. Liang, Z. Zhang, M. Ge, G. Xing and G. Sun, *Small*, 2021, **17**, e2103514.

107 J.-C. Blancon, H. Tsai, W. Nie, C. C. Stoumpos, L. Pedesseau, C. Katan, M. Kepenekian, C. M. M. Soe, K. Appavoo, M. Y. Sfeir, S. Tretiak, P. M. Ajayan, M. G. Kanatzidis, J. Even, J. J. Crochet and A. D. Mohite, *Science*, 2017, **355**, 1288–1292.

108 A. Swarnkar, A. R. Marshall, E. M. Sanehira, B. D. Chernomordik, D. T. Moore, J. A. Christians, T. Chakrabarti and J. M. Luther, *Science*, 2016, **354**, 92–95.

109 B. Turedi, M. N. Lintangpradipto, O. J. Sandberg, A. Yazmaciyan, G. J. Matt, A. Y. Alsalloum, K. Almasabi, K. Sakhatskyi, S. Yakunin, X. Zheng, R. Naphade, S. Nematulloev, V. Yeddu, D. Baran, A. Armin, M. I. Saidaminov, M. V. Kovalenko, O. F. Mohammed and O. M. Bakr, *Adv. Mater.*, 2022, **34**, e2202390.